Interplay between numerical relativity and black hole perturbation theory in the intermediate-mass-ratio regime

Tousif Islam[*]

Department of Physics, University of Massachusetts, Dartmouth, Massachusetts 02747, USA;
Department of Mathematics, University of Massachusetts, Dartmouth, Massachusetts 02747, USA;
and Center for Scientific Computing and Visualization Research, University of Massachusetts,
Dartmouth, Massachusetts 02747, USA

We investigate the interplay between numerical relativity (NR) and point-particle black hole perturbation theory (ppBHPT) for quasi-circular nonspinning binary black holes in the intermediate mass ratio regime: $7 \leq q \leq 128$ (where $q := m_1/m_2$ is the mass ratio of the binary with m_1 and m_2 being the mass of the primary and secondary black hole respectively). Initially, we conduct a comprehensive comparison between the dominant $(\ell, m) = (2, 2)$ mode of the gravitational radiation obtained from state-of-the-art NR simulations and ppBHPT waveforms along with waveforms generated from recently developed NR-informed ppBHPT surrogate model, `BHPTNRSur1dq1e4`. This surrogate model employs a simple but nontrivial rescaling technique known as the α-β scaling to effectively match ppBHPT waveforms to NR in the comparable mass ratio regime. Subsequently, we analyze the amplitude and frequency differences between NR and ppBHPT waveforms to investigate the nonlinearities, beyond adiabatic evolution, that are present during the merger stage of the binary evolution and propose fitting functions to describe these differences in terms of both the mass ratio and the symmetric mass ratio. Finally, we assess the performance of the α-β scaling technique in the intermediate mass ratio regime.

I. INTRODUCTION

The detection and characterization of gravitational wave (GW) signals from binary black hole (BBH) mergers require computationally efficient yet accurate multimodal waveform models. The development of such models relies heavily on accurate numerical simulations of BBH mergers. The most accurate way to simulate a BBH merger is by solving the Einstein equations using numerical relativity (NR). Over the past two decades, NR pipelines have been refined for BBH systems with comparable masses $(1 \leq q \leq 10)$ [1–8]. The availability of a substantial number of NR simulations in the comparable mass ratio regime has facilitated the development of computationally efficient and accurate approximate models, such as reduced-order surrogate models based on NR data [9–14], or semianalytical models calibrated against NR simulations [15–23]. On the other hand, extreme mass ratio binaries (i.e., $q \to \infty$) can, in principle, be modeled accurately with point particle black hole perturbation theory (ppBHPT) where the smaller black hole is treated as a point particle orbiting the larger black hole in a curved space-time background. Substantial progress has been made over the past two decades in simulating BBH mergers accurately in this regime [24–33].

However, it is the intermediate mass ratio regime $(10 \leq q \leq 100)$ that still presents significant challenges for performing accurate simulations of BBH mergers. NR simulations for binaries in this mass ratio range become exceedingly computationally expensive for a variety of reasons. On the other hand, as the binary becomes less asymmetric, the assumptions of the ppBHPT framework begin to break down. Therefore, the intermediate mass ratio regime provides a unique opportunity to compare and contrast results obtained from NR and ppBHPT framework. In particular, Refs. [34–36] studied this regime to gain insights into the limitations and accuracy of both approaches as well as to further the understanding about the dynamics of the binary.

Recently, a significant milestone has been reached with the development of the `BHPTNRSur1dq1e4` surrogate model [37]. This model, based on the ppBHPT framework, accurately predicts waveforms for comparable to large mass ratio binaries. Through a simple but nontrivial calibration process, the ppBHPT waveforms are rescaled to achieve a remarkable agreement with NR data in the comparable mass ratio regime. In a parallel effort, Ref. [38] has developed a fully relativistic second-order self-force model, which also demonstrates excellent agreement with NR in the comparable mass ratio regime. Additionally, recent advancements in NR techniques have pushed the

[*]tislam@umassd.edu

boundaries of BBH simulations, enabling the simulations of BBH mergers with mass ratios up to $q = 128$ for various spin configurations [39–42]. These new NR simulations provide valuable data that can be compared with results obtained from perturbative techniques such as the ppBHPT framework (including the BHPTNRSur1dq1e4 surrogate model) and the second-order self-force model.

Building upon these recent advances, in this paper, we provide a detailed comparison between state-of-the-art NR simulations and perturbative results in the intermediate mass ratio regime. We begin by providing an executive summary of the waveform data obtained from NR and point particle black hole perturbation theory (ppBHPT) in Sec. II. In Sec. III A, we conduct a comprehensive comparison of the dominant $(\ell, m) = (2, 2)$ mode of the waveforms. We examine the phenomenology of the amplitudes and frequencies of different modes in Sec. III B and discuss the differences in peak times of various spherical harmonic modes of the gravitational radiation in Sec. III C. To understand the nonlinearities during the merger stage, we analyze the amplitude differences between NR and ppBHPT waveforms and propose fitting functions to describe these differences in Sec. IV A. Additionally, we evaluate the effectiveness of the α-β scaling technique in the intermediate mass ratio regime. We provide similar fits for the frequency differences in Sec. IV B. Finally, in Sec. V, we discuss the implications and lessons learned for both NR and perturbative techniques.

II. GRAVITATIONAL WAVEFORMS IN THE INTERMEDIATE MASS RATIO REGIME

Gravitational radiation from the merger of a binary black hole is typically written as a superposition of -2 spin-weighted spherical harmonic modes with indices (ℓ, m):

$$h(t, \theta, \phi; \lambda) = \sum_{\ell=2}^{\infty} \sum_{m=-\ell}^{\ell} h^{\ell m}(t; \lambda)_{-2} Y_{\ell m}(\theta, \phi), \quad (1)$$

where λ is the set of intrinsic parameters (such as the masses and spins of the binary) describing the system, θ is the polar angle, and ϕ is the azimuthal angle. In this paper, $h(t, \theta, \phi; \lambda)$ is obtained from both NR simulations and different flavors of perturbation theory frameworks.

a. Numerical relativity data. We utilize the latest NR simulations of high mass ratio binaries performed by the RIT group [39,40]. These simulations encompass mass ratios up to $q \leq 128$ and spins ranging from -0.85 to 0.85. The NR waveforms obtained from these simulations include modes up to $\ell = 6$. However, due to numerical noise, we restrict our analysis to modes up to $\ell = 4$ only. Additionally, for the current study, we focus exclusively on nonspinning cases.

b. Perturbation theory waveforms. We generate ppBHPT waveforms using the BHPTNRSur1dq1e4 model [37], a

recently developed surrogate waveform model that combines numerical relativity (NR) information with perturbation theory. This model can be accessed through the gwsurrogate [43] or the BHPTNRSurrogate [44] package from the Black Hole Perturbation Theory Toolkit [45].

The BHPTNRSur1dq1e4 model is trained on waveform data generated by the ppBHPT framework for nonspinning binaries with mass ratios ranging from $q = 2.5$ to $q = 10^4$. The full inspiral-merger-ringdown (IMR) ppBHPT waveform training data is computed using a time-domain Teukolsky equation solver, which has been extensively described in the literature [24–27,37,46]. The model includes a total of 50 spherical harmonic modes up to $\ell = 10$.

The model calibrates ppBHPT waveforms to NR data in the comparable mass ratio regime ($2.5 \leq q \leq 10$) up to $\ell = 5$ employing a simple but nontrivial scaling called the α-β scaling [37]:

$$h^{\ell,m}_{\text{full},\alpha_\ell,\beta}(t; q) \sim \alpha_\ell h^{\ell,m}_{\text{pp}}(t\beta; q), \quad (2)$$

where α_ℓ and β are determined by minimizing the L_2-norm between the NR and rescaled ppBHPT waveforms. After this α-β calibration step, the ppBHPT waveforms exhibit remarkable agreement with NR waveforms [with an error of $\sim 10^{-3}$ for the (2,2 mode)]. For instance, when compared to recent SXS and RIT NR simulations with mass ratios ranging from $q = 15$ to $q = 32$, the dominant quadrupolar mode of BHPTNRSur1dq1e4 agrees to NR with errors smaller than $\approx 10^{-3}$. Further studies have shown that the α-β scaling corrects for the missing finite size effect of the secondary black hole in ppBHPT framework [47].

Using BHPTNRSurrogate [44], we then generate both ppBHPT and rescaled ppBHPT waveforms for any mass ratio within the training range of the model.

III. COMPARISON BETWEEN NR AND PERTURBATION WAVEFORMS

Currently available high mass ratio NR simulations are of varying lengths, often spanning only $1500M$ (where M is the total mass of the binary). This limited duration frequently poses a challenge when conducting a detailed comparison with existing waveform models. Additionally, many of the high mass ratio simulations exhibit residual eccentricity (see the Appendix), further complicating waveform-level comparisons. Nonetheless, in Ref. [37], an interesting comparison is presented between RIT NR data and the BHPTNRSur1dq1e4 waveform model for mass ratios $q = [15, 32]$. While a comprehensive comparison of the full inspiral-merger-ringdown waveform is challenging due to the residual eccentricity in these simulations, they can still be utilized to comprehend and compare waveform phenomenology during the merger-ringdown stage, where the binary significantly circularizes. Hence, this paper

primarily focuses on comparing the phenomenology of the NR data with the waveforms obtained from perturbation theory models.

A. Comparison of $(\ell, m) = (2,2)$ mode waveforms

To begin, we decompose each spherical harmonics mode $h^{\ell m}(t)$ into its amplitude $A^{\ell m}(t)$ and phase $\phi^{\ell m}$ components, represented as $h^{\ell m}(t) = A^{\ell m}(t)e^{i\phi^{\ell m}}$.

For simplicity, we first focus on comparing the dominant $(\ell, m) = (2,2)$ mode during the final $\sim 1000M$ of the binary's evolution (see Fig. 1). To facilitate this comparison, we align the multimodal NR data (shown as solid black lines; labeled as RIT-NR), ppBHPT waveforms (shown as solid yellow lines; labeled as BHPT), and rescaled ppBHPT waveforms (represented by dashed red lines; labeled as BHPTNRSur1dq1e4) on the same time grid $t = [-1000, 100]M$, where $t = 0M$ corresponds
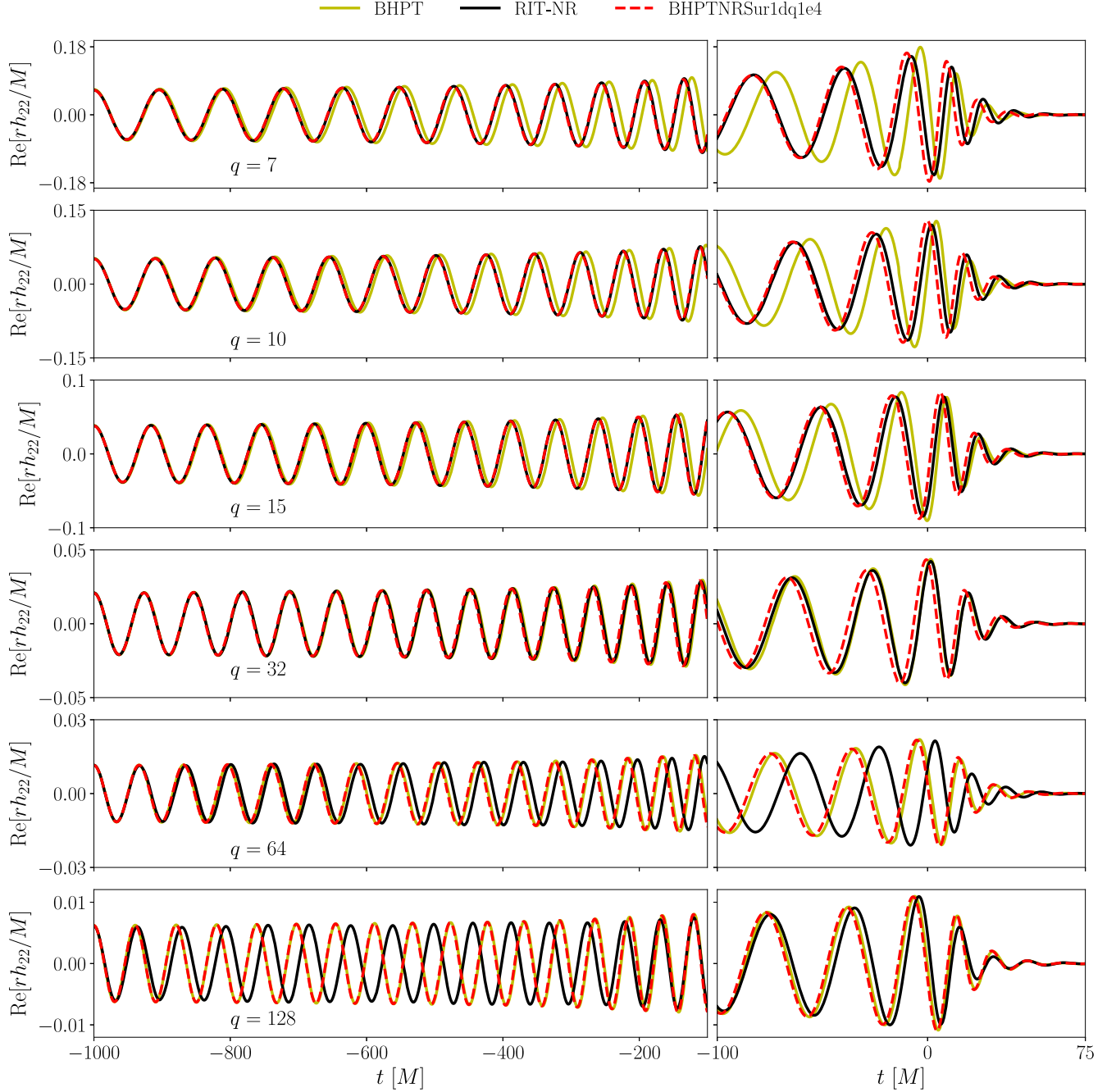

FIG. 1. We show the real part of the (2,2) mode extracted from the NR data (solid black lines; labeled as "RIT-NR"), along with the ppBHPT waveform (solid yellow lines; labeled as "BHPT") and rescaled ppBHPT waveforms generated using the `BHPTNRSur1dq1e4` model (dashed red lines; labeled as "BHPTNRSur1dq1e4") for mass ratios $q = [7, 15, 32, 64, 128]$. More details are in Sec. III A.
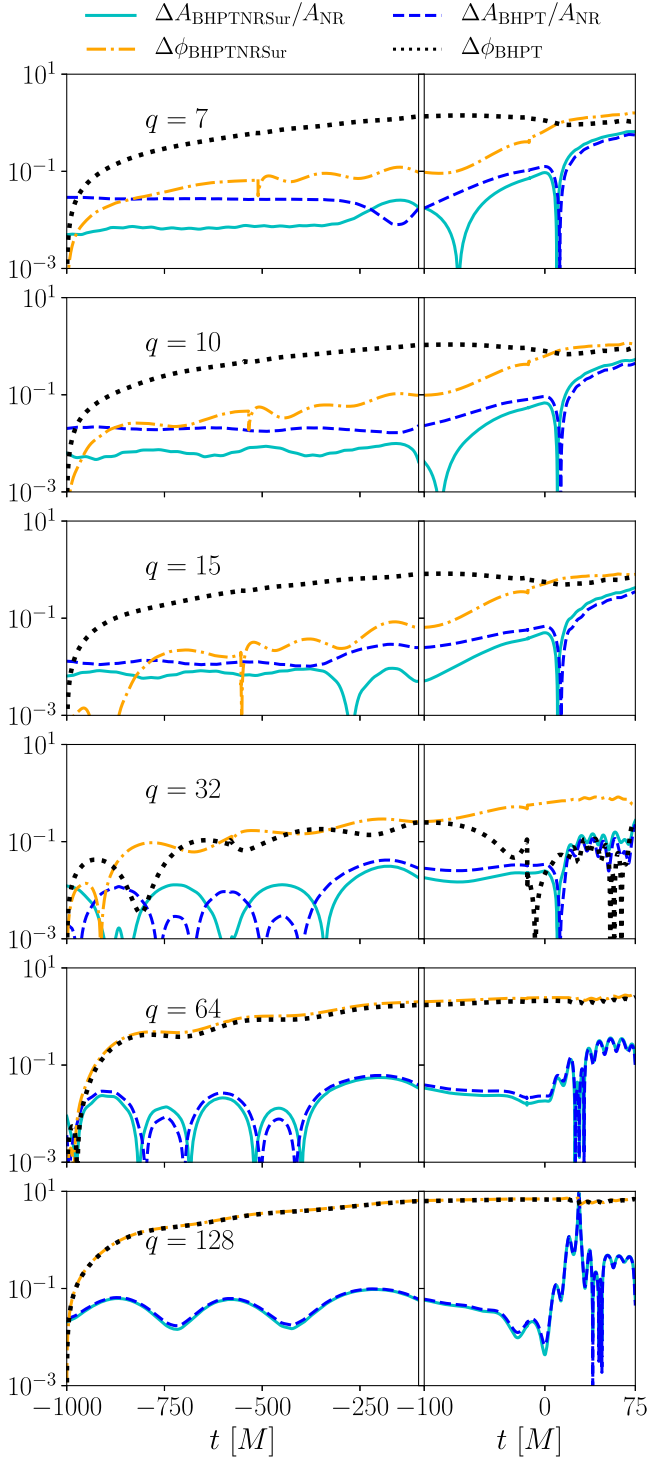
FIG. 2. We show the relative differences in amplitude $\Delta A_{22}/A_{22}^{\mathrm{NR}}$ and the absolute differences in phase $\Delta\phi_{22}$ for both ppBHPT and rescaled ppBHPT waveforms compared to the NR data for mass ratios $q = [7, 15, 32, 64, 128]$. More details are in Sec. III A.

to the peak of the $(\ell, m) = (2, 2)$ mode amplitude. Additionally, we adjust the phases such that the orbital phase is zero at the beginning of the waveforms, i.e., at $t = -1000M$.

We observe that the rescaled ppBHPT waveforms exhibit a close match to the NR data for mass ratios ranging from $q = 7$ to $q = 32$, while the ppBHPT waveforms display differences in both amplitude and phase evolution when compared to NR data (top four rows of Fig. 1). However, for mass ratios $q \geq 64$, the NR data shows notable eccentricities, resulting in significant dephasing between the ppBHPT waveforms and NR, as well as between the rescaled ppBHPT waveforms and NR (bottom three rows of Fig. 1). Furthermore, it is important to mention that the ppBHPT and rescaled ppBHPT waveforms become increasingly similar to each other for mass ratios $q \geq 64$. This suggests that the higher-order corrections to the linear ppBHPT results are relatively small in this regime.

In order to analyze the discrepancies between these waveforms, we calculate the relative differences in amplitude $\Delta A_{22}/A_{22}^{\mathrm{NR}}$ and the absolute differences in phase $\Delta\phi_{22}$ for both ppBHPT and rescaled ppBHPT waveforms compared to the NR data. Figure 2 illustrates the errors in amplitudes and phases during the late inspiral-merger-ringdown phase of the waveforms. For mass ratios in the range of $q = 7$ to $q = 16$, it is clear that the differences in both amplitudes and phases between the rescaled ppBHPT waveforms and the NR waveforms are significantly smaller than those observed between the ppBHPT waveforms and NR. This suggests that the linear ppBHPT waveforms are insufficient in accurately matching the NR waveforms within this mass ratio range. However, as we move toward higher mass ratios (i.e. $q \geq 32$), the differences in $\Delta A_{22}/A_{22}^{\mathrm{NR}}$ and $\Delta\phi_{22}$ between the ppBHPT and rescaled ppBHPT waveforms diminish gradually. This indicates that the linear description of the binary evolution becomes increasingly accurate as the mass ratio increases. For mass ratios $q \geq 64$, both $\Delta A_{22}/A_{22}^{\mathrm{NR}}$ and $\Delta\phi_{22}$ exhibit distinct features that strongly suggest the presence of residual eccentricities in the NR simulations.

At this point, we aim to quantify the difference between NR and (scaled) ppBHPT waveforms for different mass ratios using the L_2-norm. To compute the L_2-norm between two waveforms $h_1^{22}(t)$ and $h_2^{22}(t)$, we minimize the time-domain overlap integral (or L_2-norm error) given by:

$$\mathcal{E}(h_1, h_2) = \min_{t_c, \varphi_z} \frac{\int |\mathrm{e}^{-2\pi i \varphi_z} h_1^{22}(t - t_c) - h_2^{22}(t)|^2 dt}{\int |h_2^{22}(t)|^2 dt}. \quad (3)$$

We compute this error over a shift in time t_c and a rotation about the z-axis by an angle φ_z. It is important to note that the duration of NR simulations varies significantly for different mass ratios. For instance, at $q = 7$, the NR data covers the final $\sim 2400M$ of the binary evolution, while for $q = 64$, the NR data is only $\sim 1000M$ long. Initially, we use all available NR data to compute these differences. We find that the scaled ppBHPT waveforms (obtained from `BHPTNRSur1dq1e4`) yield a better match to NR than the original ppBHPT waveforms. For example, the L_2-norm
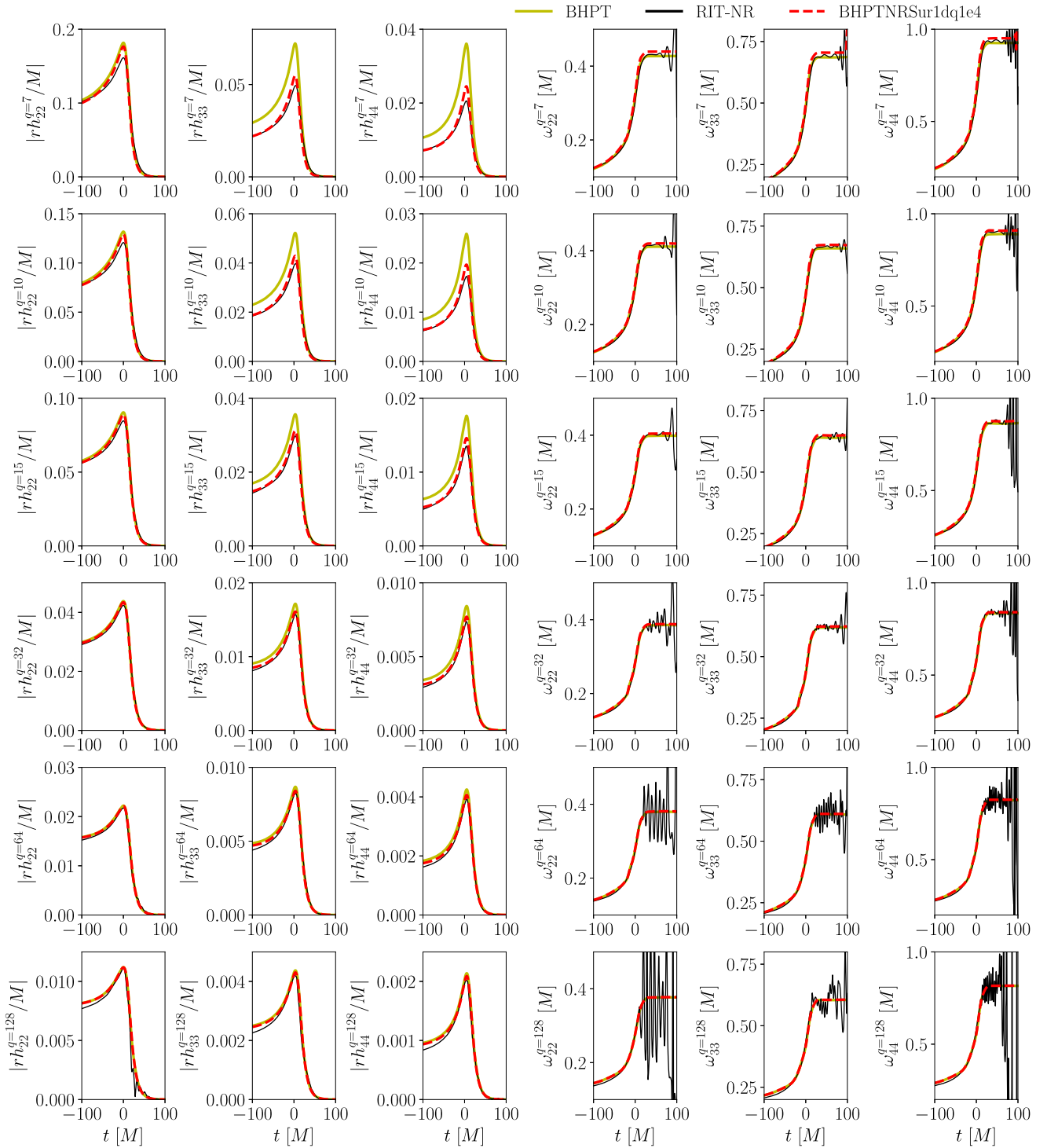
FIG. 3. We show the amplitudes and instantaneous frequencies of the (2,2), (3,3), and (4,4) spherical harmonic modes extracted from the NR data (solid black lines), along with the amplitudes and instantaneous frequencies obtained from the ppBHPT waveforms (solid yellow lines; labeled as "BHPT") and rescaled ppBHPT waveforms generated using the `BHPTNRSur1dq1e4` model (dashed red lines; labeled as "BHPTNRSur1dq1e4") for mass ratios $q = [7, 15, 32, 64, 128]$. More details are in Sec. III A.

error between NR and ppBHPT waveforms is ∼0.6, while the error between NR and scaled ppBHPT waveforms is ∼0.03 for $q = 10$. However, for $q = 64$, both ppBHPT and scaled ppBHPT waveforms exhibit equally worse agreement with

NR data (which includes residual eccentricity), yielding L_2-norm values of 0.6 and 0.7, respectively. Similar errors are also obtained for $q = 128$. We further point out that the errors are worse for the higher order modes.

B. Comparison of the amplitudes and frequencies of different modes

We now examine the amplitudes and instantaneous frequencies of three representative modes $[(\ell, m)] = [(2, 2), (3, 3), (4, 4)]$ for mass ratios ranging from $q = 7$ to $q = 128$ (see Fig. 3). For any given mode, instantaneous frequencies $\omega_{\ell,m}$ is given by the time derivative of the phase

$$\omega_{\ell,m} = \frac{d\phi_{\ell,m}}{dt}. \tag{4}$$

To mitigate the impact of residual eccentricities in the comparisons, we focus on the merger-ringdown stage of the binary ($-100M \leq t \leq 100M$), where circularization is expected to be nearly complete. For mass ratios $7 \leq q \leq 32$, noticeable differences are observed between ppBHPT and NR amplitudes, while the rescaled ppBHPT amplitudes closely match the NR values across all mass ratios. Moreover, as anticipated, the differences in amplitudes between ppBHPT and NR (and rescaled ppBHPT) decrease as the mass ratio increases. For $q \geq 64$, ppBHPT and rescaled ppBHPT produce nearly identical amplitudes. Interestingly, the frequencies of the individual modes computed from ppBHPT waveforms and NR exhibit remarkable agreements for all mass ratios. It is important to note that due to numerical noise in the NR data, frequencies display unphysical oscillations after the merger, particularly for mass ratios $q \geq 15$.

C. Comparison of the peak times

Next, we determine the times $t_{\ell,m}^{\text{peak}}$ corresponding to the maximum amplitude $A^{\text{peak}}\ell, m$ for each spherical harmonic mode. We then calculate the relative time of the peaks with respect to the dominant (2,2) mode as:

$$\delta t^{\text{peak}}\ell, m = t_{\ell,m}^{\text{peak}} - t_{2,2}^{\text{peak}}, \tag{5}$$

where $t_{2,2}^{\text{peak}}$ is the time at which the (2,2) mode amplitude reaches its maximum. We show the relative peak times $\delta t_{\ell,m}^{\text{peak}}$ in the NR data for a set of three representative modes $[(\ell, m)] = [(2, 1), (3, 3), (4, 4)]$ along with the relative peak times for the same modes in the ppBHPT and rescaled ppBHPT waveforms in Fig. 4. For comparison, we include the relative peak times of these modes from one of the state-of-the-art effective-one-body models for aligned-spin binaries, namely SEOBNRv4HM. This model includes four higher-order modes in addition to the dominant quadrupolar mode of radiation: $(\ell, m) = [(2, \pm 1), (3, \pm 3), (4, \pm 4), (5, \pm 5)]$, and it is calibrated to a set of 141 NR waveforms for mass ratios $q \leq 10$ and spins $\chi_{1,2} \leq 0.99$.

Interestingly, the relative peak times $\delta t_{\ell,m}^{\text{peak}}$ within these waveforms exhibit significant inconsistencies with each other for almost all mass ratio values. The inconsistencies in the relative peak times $\delta t_{\ell,m}^{\text{peak}}$ indicate that there is still room for improvement in accurately predicting the timing of
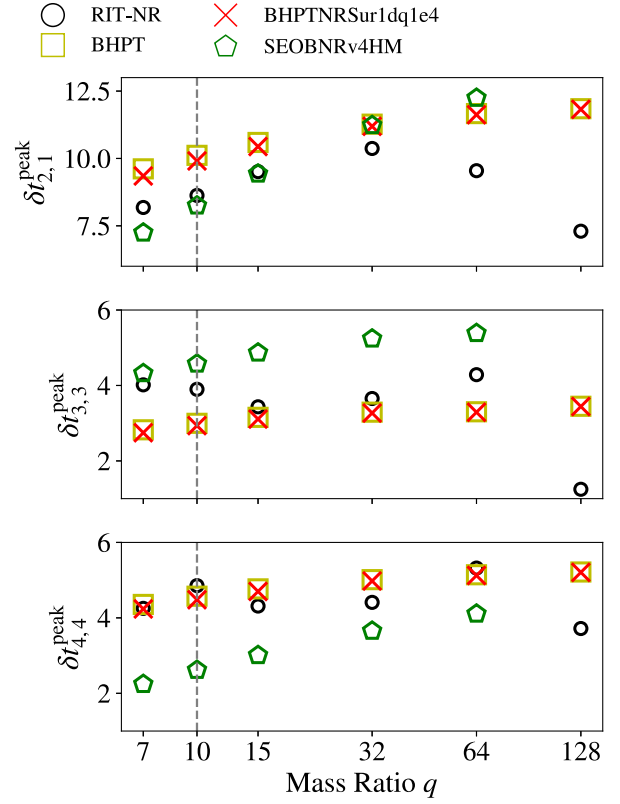

FIG. 4. We show the relative times (with respect to the (2,2) mode) at which the amplitudes of the (2,1) mode (upper panel), (3,3) mode (middle panel), and (4,4) mode (lower panel) reach the maximum in the NR data (circles) along with the times obtained from the ppBHPT waveforms (squares; labeled as BHPT) and rescaled ppBHPT waveforms generated using the BHPTNRSur1dq1e4 model (crosses; labeled as BHPTNRSur1dq1e4). Additionally, we include the relative peak locations in the SEOBNRv4HM model (represented by pentagons) for comparison. The gray vertical dashed line represents $q = 10$, which serves as a crude boundary between the comparable mass regime and the intermediate mass ratio regime. More details are in Sec. III C.

different modes during the merger-ringdown phases of binary black hole systems. Further developments in waveform modeling techniques and more comprehensive calibration against NR simulations may help reduce the discrepancies. We further notice that the differences in peak times between ppBHPT and rescaled ppBHPT waveforms are very small. This can be attributed to the dominant influence of the inspiral phase in the α-β calibration procedure. Accurate modeling of the peak times in rescaled ppBHPT waveforms (i.e. in BHPTNRSur1dq1e4) may require further tuning in the merger-ringdown part as done in Ref. [48].

IV. INTERPLAY BETWEEN NR AND PERTURBATION THEORY

To gain a deeper understanding of the interaction between the NR and ppBHPT waveforms, we now examine

their disparities in terms of amplitude and frequencies (as illustrated in Fig. 3) across different mass ratios.

A. Amplitude differences between NR and ppBHPT

We first investigate the differences between NR and ppBHPT in amplitude across various mass ratios. Specifically, we replicate and expand upon the analysis presented in Refs. [34–36]. Following the methodology outlined in Refs. [34–36], we define the amplitude differences as:

$$\delta A_{\ell,m} = |A_{\ell,m}^{\text{BHPT}} - A_{\ell,m}^{\text{NR}}|, \tag{6}$$

where $A_{\ell,m}^{\text{BHPT}}$ represents the amplitude of the ppBHPT waveform.

We observe that the amplitude differences for the $q = 10$ and $q = 15$ cases near the merger exhibit the following behavior (Fig. 5):

$$\delta A_{22}^{q=10} \sim 1.92 \times \delta A_{22}^{q=15}$$
$$\sim 1.44^{1.92} \times \delta A_{22}^{q=15}, \tag{7}$$

where 1.44 is to the ratio of the symmetric mass ratios ν. This approximate scaling differs slightly from the one reported in Ref. [36], which suggested $\delta A_{22}^{q=10} \sim 1.44^{2.3} \times \delta A_{22}^{q=15}$. Nevertheless, both results indicate the presence of nonlinear effects (beyond adiabatic evolution) in the amplitude differences between the NR and ppBHPT waveforms, as these differences scale nonlinearly with
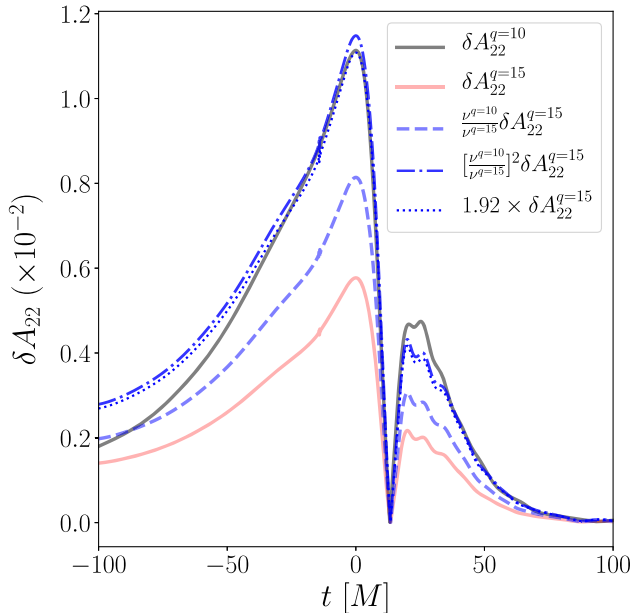
the symmetric mass ratio ν. Likewise, we find that the amplitude differences for the $q = 10$ and $q = 32$ cases near the merger can be characterized as follows:

$$\delta A_{22}^{q=10} \sim 7.7 \times \delta A_{22}^{q=32}$$
$$\sim 2.81^{1.98} \times \delta A_{22}^{q=32}, \tag{8}$$

where 2.81 is the ratio of the symmetric mass ratios ν. Similarly, the amplitude differences for the $q = 15$ and $q = 32$ cases near the merger obeys:

$$\delta A_{22}^{q=10} \sim 3.97 \times \delta A_{22}^{q=32}$$
$$\sim 1.99^{1.96} \times \delta A_{22}^{q=32}, \tag{9}$$

where 1.99 is the ratio of the symmetric mass ratios ν.

Next, we perform fitting for the amplitude differences $\delta A_{\ell,m}$ of three representative modes $(\ell, m) = [(2,2), (3,3), (4,4)]$ at their respective peaks as a function of ν (Fig. 6). The obtained relations are as follows:

$$\delta A_{2,2} \sim 6.07 \times \nu^{3.06} \tag{10}$$

$$\delta A_{3,3} \sim 1.53 \times \nu^{2.90} \tag{11}$$

$$\delta A_{4,4} \sim 0.43 \times \nu^{2.84}. \tag{12}$$

Next, we repeat the fitting in terms of $\frac{1}{q}$ [(Fig. 7)] and find:

FIG. 5. We show the amplitude difference δA_{22} between ppBHPT and NR for $q = 10$ (solid gray line) and $q = 15$ (solid red line). Furthermore, we show the amplitude difference for $q = 15$ after rescaling them with different powers of the ratio of symmetric mass ratios (blue lines). More details are in Sec. IV A.
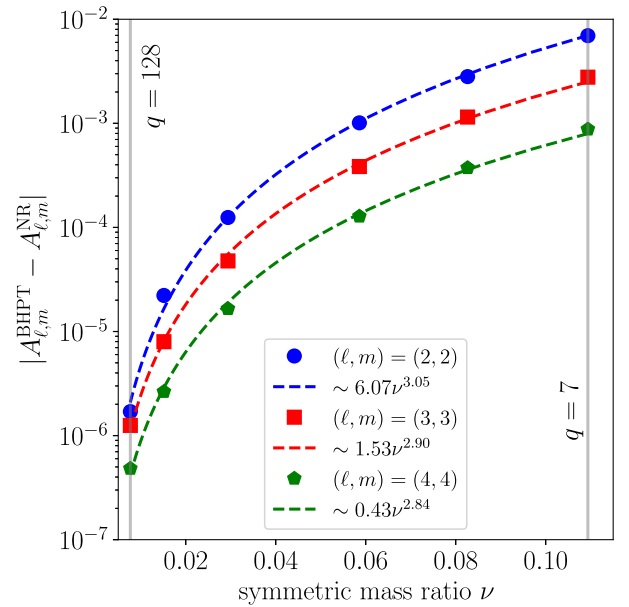

FIG. 6. We show the amplitude differences $\delta A_{\ell,m}$ between ppBHPT and NR data at the merger (denoted by the maximum amplitude in the (2,2) mode) for (2,2) (blue circles), (3,3) (red squares) and (4,4) (green pentagons) modes for mass ratios $q = [7, 15, 32, 64, 128]$. Additionally, we show the best-fit functions for each mode in terms of ν. More details are in Sec. IV A.
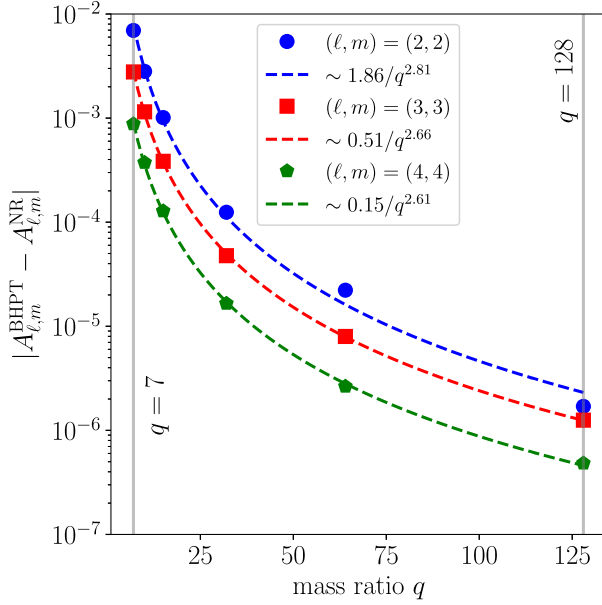
FIG. 7. We show the amplitude differences $\delta A_{\ell,m}$ between ppBHPT and NR data at the merger (denoted by the maximum amplitude in the (2,2) mode) for (2,2) (blue circles), (3,3) (red squares), and (4,4) (green pentagons) modes for mass ratios $q = [7, 15, 32, 64, 128]$. Additionally, we show the best-fit functions for each mode in terms of $\frac{1}{q}$. More details are in Sec. IV A.

$$\delta A_{2,2} \sim 1.86/q^{2.81} \qquad (13)$$

$$\delta A_{3,3} \sim 0.51/q^{2.66} \qquad (14)$$

$$\delta A_{4,4} \sim 0.15/q^{2.61}. \qquad (15)$$

These fits not only provide a simple scaling for the differences in maximum amplitudes between ppBHPT and NR waveforms, but also serve as further confirmation of the presence of nonlinearity during the merger stage of the binary evolution. Additionally, we observe that the nonlinearity is more pronounced in the (2,2) mode compared to higher order modes.

We now calculate A_{NR}/A_{BHPT}, which represents the ratio of the ppBHPT and NR amplitudes for all mass ratios. This ratio is expected to correspond roughly to the α parameter in Eq. (2) after multiplying by the transformation factor $\frac{1}{1+1/q}$ between a mass scale of m_1 and M. In Fig. 8, we present both the ratio of the amplitude A_{NR}/A_{BHPT} and the α values obtained from the BHPTNRSur1dq1e4 model. We observe that as the mass ratio increases, the agreement between these two quantities improves, suggesting that the α-β scaling works reasonably well even beyond the comparable mass ratio regime where it was originally constructed. The differences observed for $q \leq 15$ can be attributed to numerical noise and the presence of residual eccentricities in the NR data.
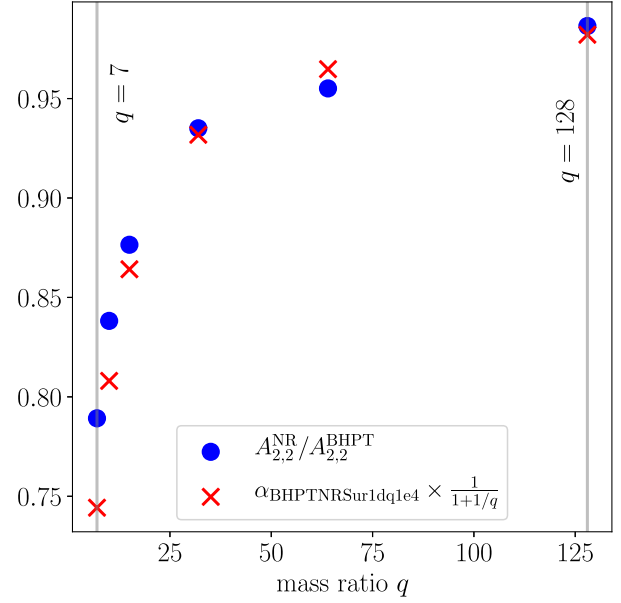
FIG. 8. We show the ratio of the ppBHPT and NR amplitudes for mass ratios $q = [7, 15, 32, 64, 128]$, along with the α parameter extracted from the BHPTNRSur1dq1e4 model. More details are in Sec. IV A.

Next, we repeat our study using scaled ppBHPT waveforms (obtained from the BHPTNRSur1dq1e4 model). In particular, we calculate the differences in amplitude across various mass ratios.

$$\delta A_{\ell,m}^{\text{scaled}} = |A_{\ell,m}^{\text{BHPTNRSur1dq1e4}} - A_{\ell,m}^{\text{NR}}|, \qquad (16)$$

where $A_{\ell,m}^{\text{BHPTNRSur1dq1e4}}$ represents the amplitude of the scaled ppBHPT waveform. At the peak, we find the following relations:

$$\delta A_{2,2}^{\text{scaled}} \sim 4.87 \times \nu^{3.09} \qquad (17)$$

$$\delta A_{3,3}^{\text{scaled}} \sim 0.13 \times \nu^{2.53} \qquad (18)$$

$$\delta A_{4,4}^{\text{scaled}} \sim 0.03 \times \nu^{2.46} \qquad (19)$$

and

$$\delta A_{2,2}^{\text{scaled}} \sim 1.47/q^{2.83} \qquad (20)$$

$$\delta A_{3,3}^{\text{scaled}} \sim 0.05/q^{2.33} \qquad (21)$$

$$\delta A_{4,4}^{\text{scaled}} \sim 0.014/q^{2.26}. \qquad (22)$$

It is worth noting that the exponents in the relation for $\delta A_{\ell,m}^{\text{scaled}}$ have changed only slightly compared to $\delta A_{\ell,m}$. However, it is important to highlight that the coefficients for $\delta A_{\ell,m}^{\text{scaled}}$ are much smaller than the ones that appear in $\delta A_{\ell,m}$.

B. Frequency differences between NR and ppBHPT

Following the methodology described in Sec. IV A regarding the amplitudes, we define the frequency differences as:

$$\delta\omega_{\ell,m} = |\omega_{\ell,m}^{\text{BHPT}} - \omega_{\ell,m}^{\text{NR}}|, \tag{23}$$

where $\omega_{\ell,m}^{\text{BHPT}}$ and $\omega_{\ell,m}^{\text{NR}}$ represent the instantaneous frequencies of the ppBHPT and NR waveforms, respectively.

We calculate $\delta\omega_{\ell,m}$ at the merger, indicated by the maximum amplitude in the (2,2) mode, for the (2,2), (3,3), and (4,4) modes for mass ratios $q = [7, 15, 32, 64, 128]$ (Fig. 9). Subsequently, we conduct a fitting analysis for the frequency differences $\delta A_{2,2}$ in terms of $\frac{1}{q}$ and obtain the following relationship (Fig. 9):

$$\delta\omega_{2,2} \sim 0.047/q^{0.73}. \tag{24}$$

Next, we repeat the fitting in terms of ν and find:

$$\delta\omega_{2,2} \sim 0.063\nu^{0.78}. \tag{25}$$

It is important to acknowledge that due to numerical noise present in the NR data, as observed in Fig. 3, it becomes increasingly difficult to obtain accurate estimates of the instantaneous frequencies from NR for mass ratios $q \geq 16$. Therefore, we refrain from attempting to fit the

frequency differences for the (3,3) and (4,4) modes in this scenario.

We then investigate the differences in the instantaneous frequencies between scaled ppBHPT and NR around merger, defined as:

$$\delta\omega_{2,2}^{\text{scaled}} = |\omega_{2,2}^{\text{BHPTNRSur1dq1e4}} - \omega_{2,2}^{\text{NR}}|. \tag{26}$$

We find the following scalings for $\delta\omega_{2,2}^{\text{scaled}}$:

$$\delta\omega_{2,2}^{\text{scaled}} \sim 0.233/q^{1.07}, \tag{27}$$

and

$$\delta\omega_{2,2}^{\text{scaled}} \sim 0.154\nu^{0.98}. \tag{28}$$

In contrast to the amplitude differences, we observe that both the coefficient and exponent are significantly different between $\delta\omega_{2,2}^{\text{scaled}}$ and $\delta\omega_{2,2}$ scalings.

V. DISCUSSIONS AND CONCLUSION

In this work, we have conducted a detailed comparison between state-of-art NR simulations and perturbative results in the intermediate mass ratio regime. In particular, we use both ppBHPT waveforms and rescaled ppBHPT waveforms from the `BHPTNRSur1dq1e4` surrogate model.

We first provide a comprehensive comparison of the dominant $(\ell, m) = (2, 2)$ mode of the gravitational radiation obtained from NR and ppBHPT techniques. We observe that the rescaled ppBHPT waveforms exhibit a close match to the NR data for mass ratios ranging from $q = 7$ to $q = 32$, while the ppBHPT waveforms display differences in both amplitude and phase evolution when compared to NR data. For mass ratios $q \geq 32$, residual eccentricities and numerical noise in the NR data make such comparisons challenging (Sec. III A; Figs. 1 and 2). We further observe that as the mass ratio increases, the differences between NR data and ppBHPT results reduce (Sec. III A; Fig. 3). Furthermore, excellent match between NR amplitudes and scaled ppBHPT amplitudes indicate effectiveness of the α-β scaling in the intermediate mass ratio regime (Sec. IV A; Fig. 8). However, the differences in peak times of different modes between NR, ppBHPT and `BHPTNRSur1dq1e4` highlight the intricacies of the merger stage, revealing insights into the nonlinear dynamics of the binary evolution (Sec. III C; Fig. 4).

Next, we examine the disparities between NR and ppBHPT waveforms in terms of amplitude and frequencies to gain a comprehensive understanding of the intricate relationship between these two frameworks. We analyze the amplitude differences $\delta A_{\ell,m}$ between NR and ppBHPT waveforms for different modes to investigate the nonlinearities present during the merger stage of the binary
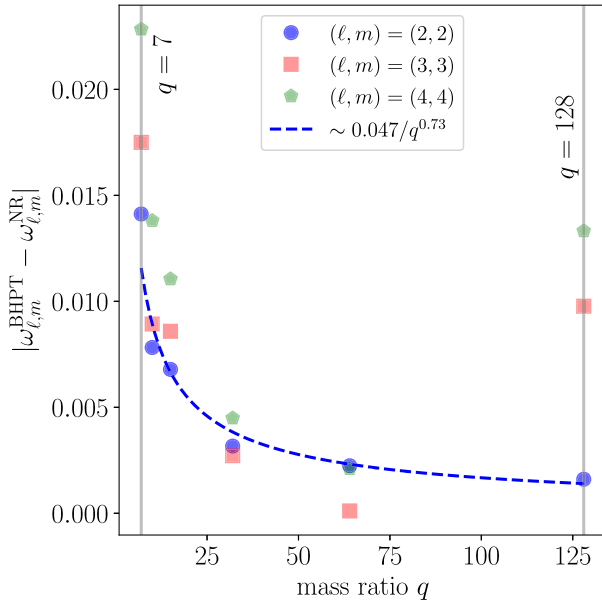

FIG. 9. We show the frequency differences $\delta\omega_{\ell,m}$ between ppBHPT and NR data at the merger (denoted by the maximum amplitude in the (2,2) mode) for (2,2) (blue circles), (3,3) (red squares), and (4,4) (green pentagons) modes for mass ratios $q = [7, 15, 32, 64, 128]$. Additionally, we show the best-fit functions for the (2,2) mode in terms of $\frac{1}{q}$. More details are in Sec. IV B.

evolution and propose fitting functions to describe these amplitude differences in terms of both q and ν. The proposed fitting functions for amplitude differences between NR and ppBHPT waveforms offer a valuable tool for understanding and quantifying these nonlinearities (Sec. IV A; Figs. 5–6). Finally, we provide similar fits for the frequency differences in the (2,2) mode in Sec. IV B.

This study highlights the potential of ppBHPT and surrogate models, such as BHPTNRSur1dq1e4, in efficiently and accurately predicting waveforms in the intermediate mass ratio regime. It opens up new opportunities for exploring the nonlinearities during the merger stage of binary and for developing reliable modeling strategies to accurately determine the peak times of each mode. Our findings underscore the importance of improving calibration methods for ppBHPT-based surrogate models and enhancing eccentricity reduction algorithms in NR simulations. These advancements will contribute to the development of more accurate and efficient waveform models, enabling better detection and characterization of GW signals in the intermediate mass ratio regime.

ACKNOWLEDGMENTS

APPENDIX: RESIDUAL ECCENTRICITIES IN RIT-NR SIMULATIONS

It is important to highlight the challenges associated with using RIT NR simulations [39,40] to estimate the accuracy of waveform models in the intermediate mass ratio regime. Two notable limitations are the shorter length of the NR data and the presence of residual eccentricities.

To illustrate these issues, we plot the amplitudes of the (2,2) mode in RIT-NR waveform data in Fig. 10 for three different mass ratios: $q = 32$ (RIT-BBH-0792; upper panel), $q = 64$ (RIT-BBH-1916; middle panel), and $q = 128$ (RIT-BBH-1076; lower panel). We have chosen the same time-range for all three subplots to stress the varying (and relatively short) length of the NR data corresponding to different mass ratios. Figure 10 further shows clear
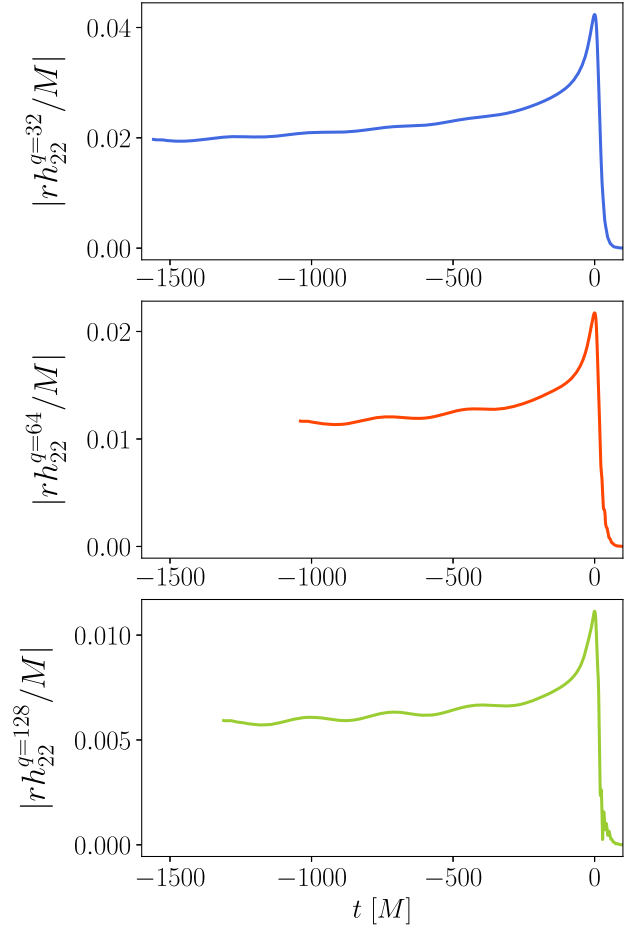

FIG. 10. We show the amplitudes of the (2,2) mode in RIT-NR waveform data for three different mass ratios: $q = [32, 64, 128]$. In all cases, we see modulations in the amplitudes due to residual eccentricity. More details are in the Appendix.

indications of residual eccentricity in the waveforms, especially for mass ratios $q = 64$ and $q = 128$. However, the metadata for these NR simulations does not provide any estimate of initial eccentricities. While it is possible to estimate eccentricities using waveform amplitude or frequencies at the periastron and apostron [14,49], the shorter duration of the NR data poses significant challenges in obtaining accurate estimates. These methods rely on precise interpolation of the frequencies at the periastron and apostron, which is difficult to achieve in cases where the NR data is limited. For example, we could only find about three apostron and periastron before merger for $q = 128$. Consequently, we could not provide any quantitative measurement of the eccentricities.

These limitations should be considered when comparing and validating models in the intermediate mass ratio range using RIT NR data.

[1] Abdul H. Mroue *et al.*, Catalog of 174 Binary Black Hole Simulations for Gravitational Wave Astronomy, Phys. Rev. Lett. **111,** 241104 (2013).

[2] Michael Boyle *et al.*, The SXS Collaboration catalog of binary black hole simulations, Classical Quantum Gravity **36,** 195006 (2019).

[3] James Healy, Carlos O. Lousto, Yosef Zlochower, and Manuela Campanelli, The RIT binary black hole simulations catalog, Classical Quantum Gravity **34,** 224001 (2017).

[4] James Healy, Carlos O. Lousto, Jacob Lange, Richard O'Shaughnessy, Yosef Zlochower, and Manuela Campanelli, Second RIT binary black hole simulations catalog and its application to gravitational waves parameter estimation, Phys. Rev. D **100,** 024021 (2019).

[5] James Healy and Carlos O. Lousto, Third RIT binary black hole simulations catalog, Phys. Rev. D **102,** 104018 (2020).

[6] James Healy and Carlos O. Lousto, Fourth RIT binary black hole simulations catalog: Extension to eccentric orbits, Phys. Rev. D **105,** 124010 (2022).

[7] Karan Jani, James Healy, James A. Clark, Lionel London, Pablo Laguna, and Deirdre Shoemaker, Georgia tech catalog of gravitational waveforms, Classical Quantum Gravity **33,** 204001 (2016).

[8] Eleanor Hamilton *et al.*, A catalogue of precessing black-hole-binary numerical-relativity simulations, arXiv:2303 .05419.

[9] Jonathan Blackman, Scott E. Field, Chad R. Galley, Béla Szilágyi, Mark A. Scheel, Manuel Tiglio, and Daniel A. Hemberger, Fast and Accurate Prediction of Numerical Relativity Waveforms from Binary Black Hole Coalescences Using Surrogate Models, Phys. Rev. Lett. **115,** 121102 (2015).

[10] Jonathan Blackman, Scott E. Field, Mark A. Scheel, Chad R. Galley, Christian D. Ott, Michael Boyle, Lawrence E. Kidder, Harald P. Pfeiffer, and Béla Szilágyi, Numerical relativity waveform surrogate model for generically precessing binary black hole mergers, Phys. Rev. D **96,** 024058 (2017).

[11] Jonathan Blackman, Scott E. Field, Mark A. Scheel, Chad R. Galley, Daniel A. Hemberger, Patricia Schmidt, and Rory Smith, A surrogate model of gravitational waveforms from numerical relativity simulations of precessing binary black hole mergers, Phys. Rev. D **95,** 104023 (2017).

[12] Vijay Varma, Scott E. Field, Mark A. Scheel, Jonathan Blackman, Lawrence E. Kidder, and Harald P. Pfeiffer, Surrogate model of hybridized numerical relativity binary black hole waveforms, Phys. Rev. D **99,** 064045 (2019).

[13] Vijay Varma, Scott E. Field, Mark A. Scheel, Jonathan Blackman, Davide Gerosa, Leo C. Stein, Lawrence E. Kidder, and Harald P. Pfeiffer, Surrogate models for precessing binary black hole simulations with unequal masses, Phys. Rev. Res. **1,** 033015 (2019).

[14] Tousif Islam, Vijay Varma, Jackie Lodman, Scott E. Field, Gaurav Khanna, Mark A. Scheel, Harald P. Pfeiffer, Davide Gerosa, and Lawrence E. Kidder, Eccentric binary black hole surrogate models for the gravitational waveform and remnant properties: Comparable mass, nonspinning case, Phys. Rev. D **103,** 064022 (2021).

[15] Alejandro Bohé *et al.*, Improved effective-one-body model of spinning, nonprecessing binary black holes for the era of gravitational-wave astrophysics with advanced detectors, Phys. Rev. D **95,** 044028 (2017).

[16] Roberto Cotesta, Alessandra Buonanno, Alejandro Bohé, Andrea Taracchini, Ian Hinder, and Serguei Ossokine, Enriching the symphony of gravitational waves from binary black holes by tuning higher harmonics, Phys. Rev. D **98,** 084028 (2018).

[17] Roberto Cotesta, Sylvain Marsat, and Michael Pürrer, Frequency domain reduced order model of aligned-spin effective-one-body waveforms with higher-order modes, Phys. Rev. D **101,** 124040 (2020).

[18] Yi Pan, Alessandra Buonanno, Andrea Taracchini, Lawrence E. Kidder, Abdul H. Mroué, Harald P. Pfeiffer, Mark A. Scheel, and Béla Szilágyi, Inspiral-merger-ringdown waveforms of spinning, precessing black-hole binaries in the effective-one-body formalism, Phys. Rev. D **89,** 084006 (2014).

[19] Stanislav Babak, Andrea Taracchini, and Alessandra Buonanno, Validating the effective-one-body model of spinning, precessing binary black holes against numerical relativity, Phys. Rev. D **95,** 024010 (2017).

[20] Sascha Husa, Sebastian Khan, Mark Hannam, Michael Pürrer, Frank Ohme, Xisco Jiménez Forteza, and Alejandro Bohé, Frequency-domain gravitational waves from nonprecessing black-hole binaries. I. New numerical waveforms and anatomy of the signal, Phys. Rev. D **93,** 044006 (2016).

[21] Sebastian Khan, Sascha Husa, Mark Hannam, Frank Ohme, Michael Pürrer, Xisco Jiménez Forteza, and Alejandro Bohé, Frequency-domain gravitational waves from nonprecessing black-hole binaries. II. A phenomenological model for the advanced detector era, Phys. Rev. D **93,** 044007 (2016).

[22] Lionel London, Sebastian Khan, Edward Fauchon-Jones, Cecilio García, Mark Hannam, Sascha Husa, Xisco Jiménez-Forteza, Chinmay Kalaghatgi, Frank Ohme, and Francesco Pannarale, First Higher-Multipole Model of Gravitational Waves from Spinning and Coalescing Black-Hole Binaries, Phys. Rev. Lett. **120,** 161102 (2018).

[23] Sebastian Khan, Katerina Chatziioannou, Mark Hannam, and Frank Ohme, Phenomenological model for the gravitational-wave signal from precessing binary black holes with two-spin effects, Phys. Rev. D **100,** 024059 (2019).

[24] Pranesh A. Sundararajan, Gaurav Khanna, and Scott A. Hughes, Towards adiabatic waveforms for inspiral into Kerr black holes. I. A new model of the source for the time domain perturbation equation, Phys. Rev. D **76,** 104005 (2007).

[25] Pranesh A. Sundararajan, Gaurav Khanna, Scott A. Hughes, and Steve Drasco, Towards adiabatic waveforms for inspiral into Kerr black holes: II. Dynamical sources and generic orbits, Phys. Rev. D **78,** 024022 (2008).

[26] Pranesh A. Sundararajan, Gaurav Khanna, and Scott A. Hughes, Binary black hole merger gravitational waves and recoil in the large mass ratio limit, Phys. Rev. D **81,** 104009 (2010).

[27] Anil Zenginoglu and Gaurav Khanna, Null Infinity Waveforms from Extreme-Mass-Ratio Inspirals in Kerr Spacetime, Phys. Rev. X **1,** 021017 (2011).

[28] Ryuichi Fujita and Hideyuki Tagoshi, New numerical methods to evaluate homogeneous solutions of the Teukolsky equation, Prog. Theor. Phys. **112,** 415 (2004).

[29] Ryuichi Fujita and Hideyuki Tagoshi, New numerical methods to evaluate homogeneous solutions of the Teukolsky equation II. Solutions of the continued fraction equation, Prog. Theor. Phys. **113,** 1165 (2005).

[30] Shuhei Mano, Hisao Suzuki, and Eiichi Takasugi, Analytic solutions of the Teukolsky equation and their low frequency expansions, Prog. Theor. Phys. **95,** 1079 (1996).

[31] William William Thomas Throwe, High precision calculation of generic extreme mass ratio inspirals, Ph.D. thesis, Massachusetts Institute of Technology, 2010.

[32] Stephen O'Sullivan and Scott A. Hughes, Strong-field tidal distortions of rotating black holes: Formalism and results for circular, equatorial orbits, Phys. Rev. D **90,** 124039 (2014); **91,** 109901(E) (2015).

[33] Steve Drasco and Scott A. Hughes, Gravitational wave snapshots of generic extreme mass ratio inspirals, Phys. Rev. D **73,** 024027 (2006); **88,** 109905(E) (2013); **90,** 109905(E) (2014).

[34] Carlos O. Lousto, Hiroyuki Nakano, Yosef Zlochower, and Manuela Campanelli, Intermediate Mass Ratio Black Hole Binaries: Numerical Relativity meets Perturbation Theory, Phys. Rev. Lett. **104,** 211101 (2010).

[35] Carlos O. Lousto, Hiroyuki Nakano, Yosef Zlochower, and Manuela Campanelli, Intermediate-mass-ratio black hole binaries: Intertwining numerical and perturbative techniques, Phys. Rev. D **82,** 104057 (2010).

[36] Hiroyuki Nakano, Yosef Zlochower, Carlos O. Lousto, and Manuela Campanelli, Intermediate-mass-ratio black hole binaries II: Modeling trajectories and gravitational waveforms, Phys. Rev. D **84,** 124006 (2011).

[37] Tousif Islam, Scott E. Field, Scott A. Hughes, Gaurav Khanna, Vijay Varma, Matthew Giesler, Mark A. Scheel, Lawrence E. Kidder, and Harald P. Pfeiffer, Surrogate model for gravitational wave signals from nonspinning, comparable-to large-mass-ratio black hole binaries built on black hole perturbation theory waveforms calibrated to numerical relativity, Phys. Rev. D **106,** 104025 (2022).

[38] Barry Wardell, Adam Pound, Niels Warburton, Jeremy Miller, Leanne Durkan, and Alexandre Le Tiec, Gravitational Waveforms for Compact Binaries from Second-Order Self-Force Theory, Phys. Rev. Lett. **130,** 241402 (2023).

[39] Carlos O. Lousto and James Healy, Exploring the Small Mass Ratio Binary Black Hole Merger via Zeno's Dichotomy Approach, Phys. Rev. Lett. **125,** 191102 (2020).

[40] Carlos O. Lousto and James Healy, Study of the intermediate mass ratio black hole binary merger up to 1000:1 with numerical relativity, Classical Quantum Gravity **40,** 09LT01 (2023).

[41] Jooheon Yoo, Vijay Varma, Matthew Giesler, Mark A. Scheel, Carl-Johan Haster, Harald P. Pfeiffer, Lawrence E. Kidder, and Michael Boyle, Targeted large mass ratio numerical relativity surrogate waveform model for GW190814, Phys. Rev. D **106,** 044001 (2022).

[42] Matthew Giesler, Mark A. Scheel, and Saul A. Teukolsky, Numerical simulations of extreme mass ratio binary black holes (to be published).

[43] Jonathan Blackman, Scott Field, Chad Galley, and Vijay Varma, gwsurrogate, https://pypi.python.org/pypi/gwsurrogate/.

[44] Scott Field, Tousif Islam, Gaurav Khanna, Nur Rifat, and Vijay Varma, BHPTNRSurrogate, http://bhptoolkit.org/BHPTNRSurrogate/.

[45] Black hole perturbation Toolkit, bhptoolkit.org.

[46] Nur E. M. Rifat, Scott E. Field, Gaurav Khanna, and Vijay Varma, Surrogate model for gravitational wave signals from comparable and large-mass-ratio black hole binaries, Phys. Rev. D **101,** 081502 (2020).

[47] Tousif Islam and Gaurav Khanna, preceding paper, Interplay between numerical relativity and perturbation theory: Finite size effects, Phys. Rev. D **108,** 044012 (2023).

[48] Tousif Islam, Scott E. Field, and Gaurav Khanna, Remnant black hole properties from numerical-relativity-informed perturbation theory and implications for waveform modelling, arXiv:2301.07215.

[49] Md Arif Shaikh, Vijay Varma, Harald P. Pfeiffer, Antoni Ramos-Buades, and Maarten van de Meent, Defining eccentricity for gravitational wave astronomy, arXiv:2302.11257.